Photoelectrochemical Properties of Heterojunction CdTe/TiO_2 Electrodes Constructed Using Highly Ordered TiO_2 Nanotube Arrays

Jason A. Seabold,[†] Karthik Shankar,[‡] Rudeger H. T. Wilke,[‡] Maggie Paulose,[‡] Oomman K. Varghese,[‡] Craig A. Grimes,[‡] and Kyoung-Shin Choi*[,†]

Department of Chemistry, Purdue University, West Lafayette, Indiana 47907, and Department of Electrical Engineering and Materials Research Institute, The Pennsylvania State University, University Park, Pennsylvania 16802

Received April 17, 2008. Revised Manuscript Received June 18, 2008

A heterojunction CdTe/TiO_2 photoelectrode was prepared by electrochemically filling the tubes and tube-to-tube voids of a TiO_2 nanotube array with CdTe. The TiO_2 nanotube arrays used in this study were prepared by anodizing titanium films, which resulted in closely packed n-type TiO_2 tubes with an average inner pore diameter of 50 nm, wall thickness of approximately 13 nm, and length of 250−300 nm. CdTe was cathodically deposited using TiO_2 nanotubes as the working electrode at $E = -0.4$ V vs Ag/AgCl at 85 °C ($3H^+ + Cd^{2+} + HTeO_2^+ + 6e^- \rightarrow CdTe + 2H_2O$). The resulting electrodes contained three-dimensionally organized CdTe/TiO_2 junction structures with significantly enhanced junction areas. Formation of the CdTe/TiO_2 junction improved the photocurrent generation and photostability of the CdTe layer when compared with a two-dimensional CdTe layer deposited directly on a conducting substrate (i.e., fluorine-doped tin oxide). A more intimate and conformal CdTe/TiO_2 junction was formed via a new deposition technique developed in this study that promotes deposition of CdTe only in the TiO_2 tubes while minimizing deposition at the tube entrances, thus preventing pore clogging. The CdTe/TiO_2 electrodes prepared by the new technique created a longer path length for light in the CdTe layer as well as increased CdTe/TiO_2 and CdTe/electrolyte junction areas. This resulted in enhanced photon absorption and photocurrent generation, achieved using a minimal amount of CdTe.

Introduction

CdTe has shown considerable promise for building thin-film solar cells capable of a significant light to electricity conversion efficiency owing to its nearly ideal bandgap for solar terrestrial photoconversion (1.5 eV) and its high absorption coefficient.[1–3] To date, most studies on CdTe-based photoelectrodes have involved assembling solar cells based on p-type CdTe/n-type CdS heterojunctions.[1–5] In this structure, photons are mainly harvested in the CdTe layer, while the CdS serves as a window layer and accepts photon-generated holes from the CdTe layer. The efficiency of current CdTe/CdS solar cells is 16.5%, although theoretical calculations suggest that the maximum achievable efficiency for CdTe solar cells is as high as 30%, therefore leaving much room for improvement.[1–4] Considering that current CdTe solar cells are built based on a two-dimensional planar junction, [1–8] constructing a three-dimensionally structured junction may be one of the most promising and straightforward strategies to enhance the efficiency of CdTe-based photoelectrochemical cells. This will allow for more efficient charge separation at the enormously enhanced junction areas, directly increasing the light to electricity conversion ratio.

The purpose of this paper is to produce CdTe photoelectrodes possessing a highly organized three-dimensional nanojunction structure. We achieve this by using TiO_2 nanotube arrays as a substrate to deposit CdTe, filling the tubes and tube-to-tube voids. The TiO_2 nanotube arrays used in this study are prepared by anodization of titanium thin films sputter deposited on fluorine doped tin oxide (FTO) substrates, which generates closely packed arrays of n-type TiO_2 nanotubes.[9–14] The band alignment between TiO_2 and

* To whom correspondence should be addressed. E-mail: kchoi1@purdue.edu.
† Purdue University.
‡ The Pennsylvania State University.

(1) Beach, J. D.; McCandless, B. E. *MRS Bull.* **2007**, *32*, 225–229, and references therein.
(2) Birkmire, R. W.; Eser, E. *Annu. Rev. Mater. Sci.* **1997**, *27*, 625–653, and references therein.
(3) Chu, T. L.; Chu, S. S. *Solid-State Electron.* **1995**, *38*, 533–549.
(4) McGregor, S. M.; Dharmadasa, I. M.; Wadsworth, I.; Care, C. M. *Opt. Mater.* **1996**, *6*, 75.
(5) Dobson, K. D.; Visoly-Fisher, I.; Hodes, G.; Cahen, D. *Adv. Mater.* **2001**, *13*, 1495.
(6) Wu, X. *Solar Energy* **2004**, *77*, 803–814.
(7) Aramoto, T.; Kumazawa, S.; Higuchi, H.; Arita, T.; Shibutani, S.; Nishio, T.; Nakajima, J.; Tsuji, M.; Hanafusa, A.; Hibino, T.; Omura, K.; Ohyama, H.; Murozono, M. *Jpn. J. Appl. Phys* **1997**, *36*, 6304–6305.
(8) Britt, J.; Ferekides, C. *Appl. Phys. Lett.* **1993**, *62*, 2851–2852.
(9) Mor, G. K.; Shankar, K.; Paulose, M.; Varghese, O. K.; Grimes, C. A. *Nano Lett.* **2005**, *5*, 191–195.
(10) Gong, D.; Grimes, C. A.; Varghese, O. K.; Hu, W.; Singh, R. S.; Chen, Z.; Dickey, E. C. *J. Mater. Res.* **2001**, *16*, 3331–3336.
(11) Paulose, M.; Shankar, K.; Yoriya, S.; Prakasam, H. E.; Varghese, O. K.; Mor, G. K.; Latempa, T. A.; Fitzgerald, A.; Grimes, C. A. *J. Phys. Chem. B* **2006**, *110*, 16179–16184.
(12) Yoriya, S.; Prakasam, H. E.; Varghese, O. K.; Shankar, K.; Paulose, M.; Mor, G. K.; Latempa, T. A.; Grimes, C. A. *Sens. Lett.* **2006**, *4*, 334–339.

10.1021/cm8010666 CCC: $40.75
Published on Web 07/29/2008

CdTe is favorable for the transfer of photoexcited electrons from the conduction band (CB) of CdTe into the CB of TiO_2, which is beneficial for reducing the rate of electron−hole recombination in the CdTe layer.[15] Efficient electron injection from the CB of CdTe to that of TiO_2 has been demonstrated by Ernst and co-workers when a thin layer of CdTe was deposited on nanoparticulate TiO_2 electrodes.[16–18]

The distinctive advantage of using TiO_2 nanotubes to form a CdTe/TiO_2 junction is that it not only increases junction areas but also promotes unidirectional charge transport due to the one-dimensional features of the tubes. These features enable TiO_2 nanotube arrays to possess charge transport properties superior to other nanoparticulate electrodes composed of randomly oriented particles which form unorganized voids.[19–24] Due to this advantage, TiO_2 nanotube arrays have been previously used as substrates for constructing highly efficient dye-sensitized solar cells and polymer/TiO_2 hybrid solar cells. [19,22,25]

In this study, we construct CdTe/TiO_2 photoelectrodes containing a three-dimensional junction and investigate how the photoelectrochemical properties and stabilities of the CdTe layer are affected by the presence of this junction. In order to deposit a CdTe layer on nonplanar TiO_2 surfaces, we employ a solution-based electrodeposition method that can allow for a conformal coating. However, even with an electrodeposition method, forming a high quality CdTe/TiO_2 junction can be difficult to achieve, because the surface and the bottom of the TiO_2 tubes are equally conductive. In this case, deposition at the entrance of the pores occurs predominantly, because this region is favored by diffusion. This leads to clogging of the pores before the insides can be completely filled with CdTe, thus preventing full utilization of the internal surfaces of the TiO_2 tubes toward forming CdTe/TiO_2 junctions. To overcome this problem, we developed a new deposition technique that makes deposition in the tubes more favorable than deposition at the entrance of the tubes, which can be used as a general method when this type of selective deposition is desired for any mesoporous or microporous substrate. A comparison of the CdTe/TiO_2 junctions prepared by both a regular deposition technique and the new technique is made to investigate how the quality of the junction affects the optical and photoelectrochemical properties of CdTe/TiO_2 electrodes.

Experimental Section

Chemicals. All materials used in this work were of reagent grade. Cadmium sulfate hydrate ($CdSO_4 \cdot 8/3H_2O$, 99+%), tellurium dioxide (TeO_2, 99+%), and sodium sulfide (Na_2S) were purchased from Sigma Aldrich. Sulfuric acid (H_2SO_4, 50%) and sodium hydroxide (NaOH, pellets) were obtained from Mallinckrodt, and cadmium chloride ($CdCl_2$, 99.0%) was from Alfa Aesar. All solutions were prepared, and glassware was cleaned using high purity water (Millipore Milli-Q system, 18 MΩ resistivity).

Construction of TiO_2 Nanotube Arrays. Transparent nanotubes were formed on fluorine doped tin oxide (FTO) glass (Hartford Glass, Hartford, IN) by potentiostatic anodization of 500 nm thick titanium films. The titanium films were deposited on glass slides via DC sputtering, and the anodization was carried out at an applied bias of 14 V in an aqueous solution containing 0.5 volume percent HF. A detailed synthesis procedure of the TiO_2 nanotubes used in this study can be found elsewhere.[26] The resultant amorphous tubes were crystallized to anatase TiO_2 by annealing at 450 °C in oxygen ambient for 2 h. The resulting nanotubes are transparent (bandgap energy = 3.4 eV) and show n-type behavior.[27] Field emission scanning electron microscopy (FE-SEM) images indicate the nanotubes have an average inner pore diameter near 50 nm and wall thickness of approximately 13 nm and are 250−300 nm in length (Figure 1).

Electrodeposition of CdTe. A conventional three-electrode setup in an undivided cell was used (Princeton Applied Research VMP2 Multichannel Potentiostat/Galvanostat) for cathodic deposition of CdTe films ($3H^+ + Cd^{2+} + HTeO_2^+ + 6e^- \rightarrow CdTe + 2H_2O$).[28–32] Counter electrodes were prepared by e-beam evaporation of 20 nm of Ti followed by 100 nm; of Pt on cleaned glass slides. The reference electrode was an Ag/AgCl electrode in 4 M KCl solution, against which all the potentials reported here were measured. For working electrodes, either FTO or TiO_2 nanotube arrays prepared on FTO substrates were used. Deposition was carried out potentiostatically at −0.4 V versus the reference electrode. The aqueous deposition solutions consisted of 0.1 M $CdSO_4$ and 0.1 mM TeO_2 at pH 1.4 (H_2SO_4) and were maintained at 85 °C throughout the deposition.

Newly deposited electrodes were rinsed with DI water and dried under a stream of nitrogen. The annealed samples were prepared by heating at 300 °C for 45 min, with a ramp of 2 °C per minute. Some samples were also treated with $CdCl_2$ before annealing. This treatment consisted of a 2 min immersion of the as-deposited samples in a saturated $CdCl_2$/methanol solution.

Characterization. X-ray diffraction (XRD) measurements were generated using a Bruker D4 diffractometer (Cu Kα radiation). FE-SEM images were taken on an FEI Nova NanoSEM 200 at an accelerating voltage of 5 kV. SEM samples were first coated with ∼2 nm of sputtered Pt to prevent charging. A Varian Cary 300 UV−visible spectrometer was used to record UV−vis spectra.

(13) Shankar, K.; Mor, G. K.; Fitzgerald, A.; Grimes, C. A. *J. Phys. Chem. C* **2007**, *111*, 21–26.
(14) Prakasam, H. E.; Shankar, K.; Paulose, M.; Varghese, O. K.; Grimes, C. A. *J. Phys. Chem. C* **2007**, *111*, 7235–7241.
(15) Tiefenbacher, S.; Pettenkofer, C.; Jaegermann, W. *J. Appl. Phys.* **2002**, *91*, 1984–1987.
(16) Ernst, K.; Sieber, I.; Neumann-Spallart, M.; Lux-Steiner, M. C.; Könenkamp, R. *Thin Solid Films* **2000**, *361*, 213–217.
(17) Ernst, K.; Engelhardt, R.; Ellmer, K.; Kelch, C.; Muffler, H. J.; Lux-Steiner, M. C.; Könenkamp, R. *Thin Solid Films* **2001**, *387*, 26–28.
(18) Ernst, K.; Belaidi, A.; Könenkamp, R. *Semicond. Sci. Technol.* **2003**, *18*, 475–479.
(19) Mor, G. K.; Shankar, K.; Paulose, M.; Varghese, O. K.; Grimes, C. A. *Nano Lett.* **2006**, *6*, 215–218.
(20) Mor, G. K.; Varghese, O. K.; Paulose, M.; Shankar, K.; Grimes, C. A. *Sol. Energy Mater. Sol. Cells* **2006**, *90*, 2011–2075.
(21) Paulose, M.; Shankar, K.; Varghese, O. K.; Mor, G. K.; Grimes, C. A. *J. Phys. D: Appl. Phys.* **2006**, *39*, 2498–2503.
(22) Shankar, K.; Mor, G. K.; Prakasam, H. E.; Yoriya, S.; Paulose, M.; Varghese, O. K.; Grimes, C. A. *Nanotechnology* **2007**, *18*, 065707.
(23) Paulose, M.; Shankar, K.; Varghese, O. K.; Mor, G. K.; Hardin, B.; Grimes, C. A. *Nanotechnology* **2006**, *17*, 1446–1448.
(24) Zhu, K.; Neale, N. R.; Miedaner, A.; Frank, A. J. *Nano Lett.* **2007**, *7*, 69–74.
(25) Mor, G. K.; Shankar, K.; Paulose, M.; Varghese, O. K.; Grimes, C. A. *Appl. Phys. Lett.* **2007**, *91*, 152111/1–152111/3.
(26) Mor, G. K.; Varghese, O. K.; Paulose, M.; Grimes, C. A. *Adv. Funct. Mater.* **2005**, *15*, 1291–1296.
(27) Varghese, O. K.; Paulose, M.; Shankar, K.; Mor, G. K.; Grimes, C. A. *J. Nanosci. Nanotechnol.* **2005**, *5*, 1158–1165.
(28) Panicker, M. P. R.; Knaster, M.; Kroger, F. A. *J. Electrochem. Soc.* **1978**, *125*, 566–572.
(29) Duffy, N. W.; Peter, L. M.; Wang, R. L.; Lane, D. W.; Rogers, K. D. *Electrochim. Acta* **2000**, *45*, 3355–3365.
(30) Lepiller, C.; Lincot, D. *J. Electrochem. Soc.* **2004**, *151*, C348−C357.
(31) Guo, Y.; Deng, X. *Sol. Energy Mater. Sol. Cells* **1993**, *29*, 115.
(32) Uosaki, K.; Takahashi, M.; Kita, H. *Electrochim. Acta* **1984**, *29*, 279.

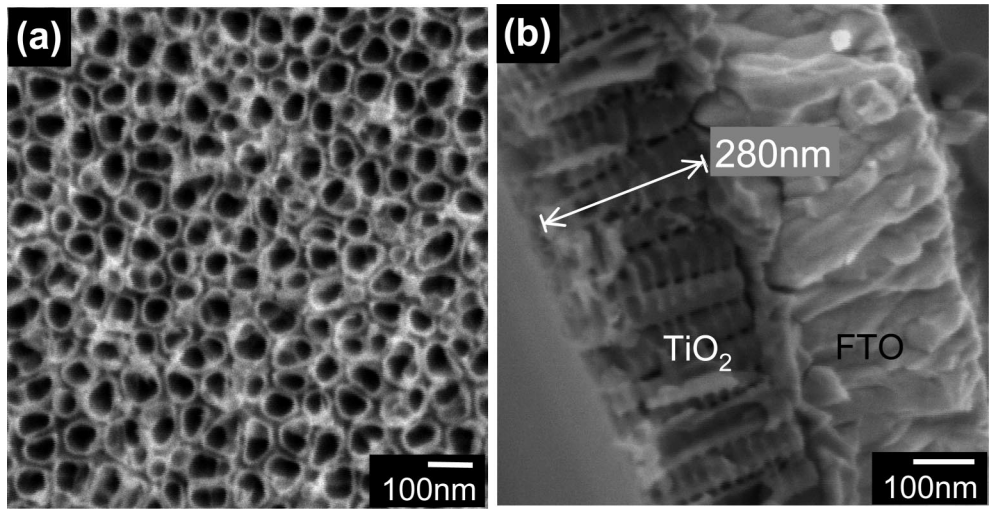

Figure 1. SEM images of TiO_2 nanotube arrays used in this study: (a) top-view and (b) side-view image.

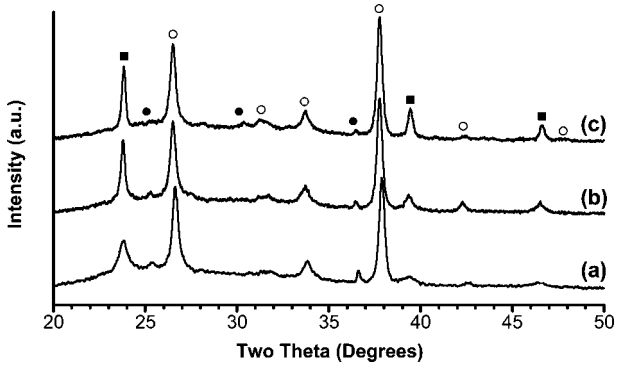

Figure 2. XRD of CdTe layers deposited on TiO_2 nanotube arrays: (a) as-deposited, (b) annealed, and (c) annealed after $CdCl_2$-treatment. Peaks generated from CdTe, TiO_2, and FTO are marked as (■), (●), and (○), respectively.

Photocurrent Measurement. Photocurrent measurements were obtained by irradiating sample films with light from a 300 W xenon arc lamp (6.0 W cm^{-2}) which had first passed through a UV filter. Measurements were conducted under a short circuit condition without applying any external bias, with output current recorded on the multichannel potentiostat. Photocurrent measurements were carried out in an aqueous electrolyte consisting of 0.6 M Na_2S, the pH of which was adjusted to 12 with addition of NaOH. Solutions were bubbled with argon for 20 min prior to use.

Results and Discussion

Figure 2a shows the X-ray diffraction pattern of a CdTe layer deposited on a TiO_2 nanotube array at −0.4 V and 85 °C for 1 h. All observed peaks can be indexed as peaks generated by CdTe, TiO_2 nanotubes, and the FTO substrate, indicating that no Cd or Te related impurities are present in the CdTe layer. The crystallinity of the CdTe layer was significantly improved by annealing the sample at 300 °C for 45 min in air (Figure 2b). The crystallinity of the CdTe films could be further improved by dipping the CdTe layer in a methanol solution saturated with $CdCl_2$ before annealing (Figure 2c). A $CdCl_2$ treatment is known for promoting recrystallization and grain growth of CdTe during the annealing process.[33–36] This process can effectively passivate defects and increase minority carrier lifetime, thereby improving device characteristics of CdTe-based solar cells (e.g., open circuit voltage and fill factor).[1,36–39]

The effect of annealing and $CdCl_2$ treatment on the CdTe layer morphology was studied by SEM (Figure 3). The as-deposited CdTe layer shows a featureless surface composed of 10−12 nm nanoparticles (Figure 3a), which become larger crystallites during the annealing process (Figure 3b). When the annealing process was combined with $CdCl_2$ treatment (Figure 3c), it resulted in the formation of larger and smoother CdTe crystals, providing evidence that $CdCl_2$ in the grain boundaries promotes grain growth during the annealing process.

UV−vis spectra of the as-deposited, annealed, and $CdCl_2$-treated and annealed CdTe layers are shown in Figure 4. While all samples show a bandgap transition at 1.48 eV, the $CdCl_2$-treated and annealed sample shows the most abrupt bandgap transition, indicating the presence of better-defined valence and conduction band edges, owing to its enhanced crystallinity and reduced surface defect sites. The as-deposited CdTe layer shows the least abrupt bandgap transition, as expected.

Photoelectrochemical properties of the CdTe/TiO_2 electrodes were characterized by measuring short-circuit photocurrent using a 0.6 M Na_2S solution with pH adjusted to 12. A UV filter was used to expose the samples only to visible light. This effectively eliminates the photocurrent contribution from the TiO_2 nanotubes and allows us to examine the photocurrent generated by only the CdTe layer. Photocurrent generated by the TiO_2 nanotubes under the conditions used in this study was less than 1 $\mu A/cm^2$.

(33) Qi, B.; Kim, D.; Williamson, D. L.; Trefny, J. U. *J. Electrochem. Soc.* **1996**, *143*, 517.
(34) Saraie, J.; Kitagawa, M.; Ishida, T.; Tanaka, J. *Crystal Growth* **1978**, *43*, 13.
(35) Levi, D. H.; Moutinho, H. R.; Hasoon, F. S.; Keyes, B. M.; Ahrenkiel, R. K.; Aljassim, M.; Kazmerski, L. L.; Birkmire, R. W. *Sol. Energy Mater. Sol. Cells* **1996**, *41*, 381.
(36) Durose, K.; Edwards, P. R.; Halliday, D. P. *J. Cryst. Growth* **1999**, *197*, 733–742.
(37) Kampmann, A.; Lincot, D. *J. Electroanal. Chem.* **1996**, *418*, 73–81.
(38) Rakhshani, A. E. *J. Appl. Phys.* **2001**, *90*, 4265–4271.
(39) Moutinho, H. R.; Al-Jassim, M. M.; Levi, D. H.; Pippo, P. C.; Kazmerski, L. L. *J. Vac. Sci. Technol.* **1998**, *A16*, 1251.

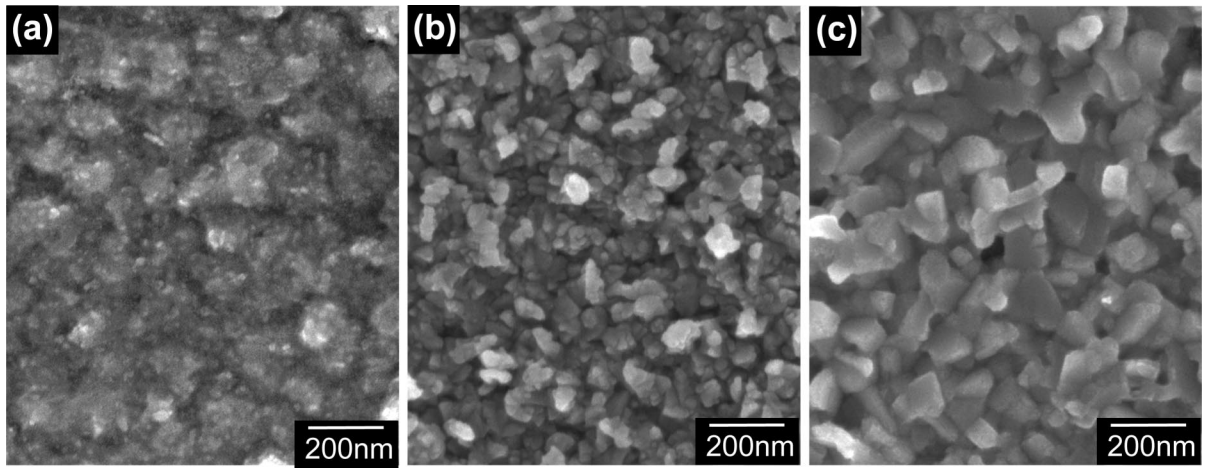

Figure 3. SEM images of CdTe layers deposited on TiO_2 nanotube arrays: (a) as-deposited, (b) annealed, and (c) annealed after $CdCl_2$ treatment.

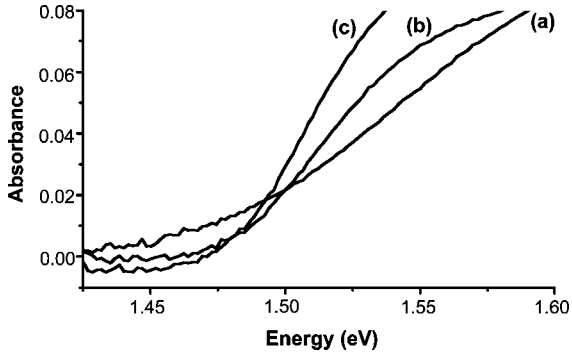

Figure 4. UV−vis spectra of CdTe layers deposited on TiO_2 nanotube arrays: (a) as-deposited, (b) annealed, and (c) annealed after $CdCl_2$ treatment.

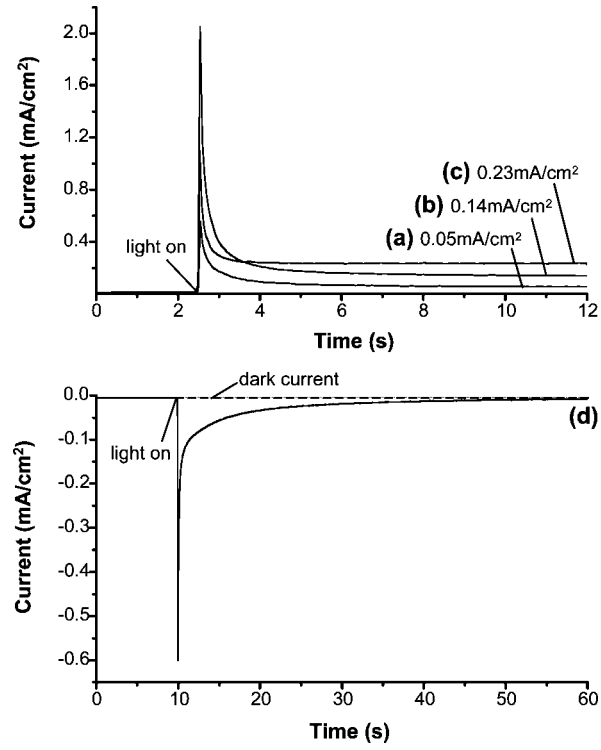

Figure 5. Short-circuit photocurrent measurement of $CdTe/TiO_2$ electrodes under visible light illumination, having CdTe layers which were (a) as-deposited, (b) annealed, and (c) annealed after $CdCl_2$ treatment. (d) Short-circuit photocurrent measurement of a CdTe layer deposited on an FTO substrate after $CdCl_2$-treatment and annealing processes.

All $CdTe/TiO_2$ electrodes (with as-deposited, annealed, and $CdCl_2$-treated and annealed CdTe layers) commonly generated anodic short-circuit photocurrent (Figure 5a−c). This means that at the CdTe/electrolyte interface the photon-generated holes are consumed to oxidize S^{2-} ions to polysulfide $(S_n)^{2-}$ ions (e.g., S_2^{2-}), while the photon-generated electrons are injected into the conduction band of TiO_2, transferred to the counter electrode, and used to reduce water to hydrogen or to reduce polysulfide ions to sulfide ions.[40] When CdTe films were deposited directly onto an FTO substrate, it showed a p-type behavior, generating cathodic photocurrent as the photon-generated electrons are predominantly consumed at the CdTe/electrolyte interface (Figure 5d).[31] This suggests that when the TiO_2/CdTe/electrolyte junction is formed, the injection of photon-generated electrons from CdTe to TiO_2 becomes more efficient than the transfer of these electrons from CdTe to the species in the electrolyte.

Among the various $CdTe/TiO_2$ electrodes, the $CdTe/TiO_2$ electrode that was $CdCl_2$-treated and annealed showed a much higher steady state photocurrent (0.23 mA/cm^2) than the as-deposited (0.05 mA/cm^2) or annealed ones (0.14 mA/cm^2; Figure 5a−c). This result agrees well with the XRD studies and UV−vis spectra of the $CdTe/TiO_2$ electrodes, where the $CdTe/TiO_2$ electrode that was $CdCl_2$-treated and annealed showed the highest crystallinity and the sharpest bandgap transition. The photocurrent of a CdTe layer deposited directly on an FTO substrate that was $CdCl_2$-treated and annealed (Figure 5d) is insignificant when compared with that of the $CdTe/TiO_2$ electrode that was equally treated (Figure 5c), which clearly demonstrates the advantages of using high surface area TiO_2 nanotubes to enhance CdTe/electrolyte junction areas. Another noticeable difference between $CdTe/TiO_2$ and CdTe electrodes is the photostability of the CdTe layer. Figure 5d shows that the photocurrent generated by a CdTe layer deposited directly on an FTO substrate gradually diminishes over time. This is most likely due to photocorrosion, which involves the anodic formation of Te ($CdTe + 2OH^- + 2p^+ \rightarrow HCdO_2^- + H^+ + Te$) and/

(40) Wrighton, M. S.; Ellis, A. B.; Kaiser, S. W. U.S. Patent 4414300, 1983.

Scheme 1. Schematic Illustration of (a) a Regular Deposition Method and (b) a Newly Developed Dipping and Deposition Technique[a]

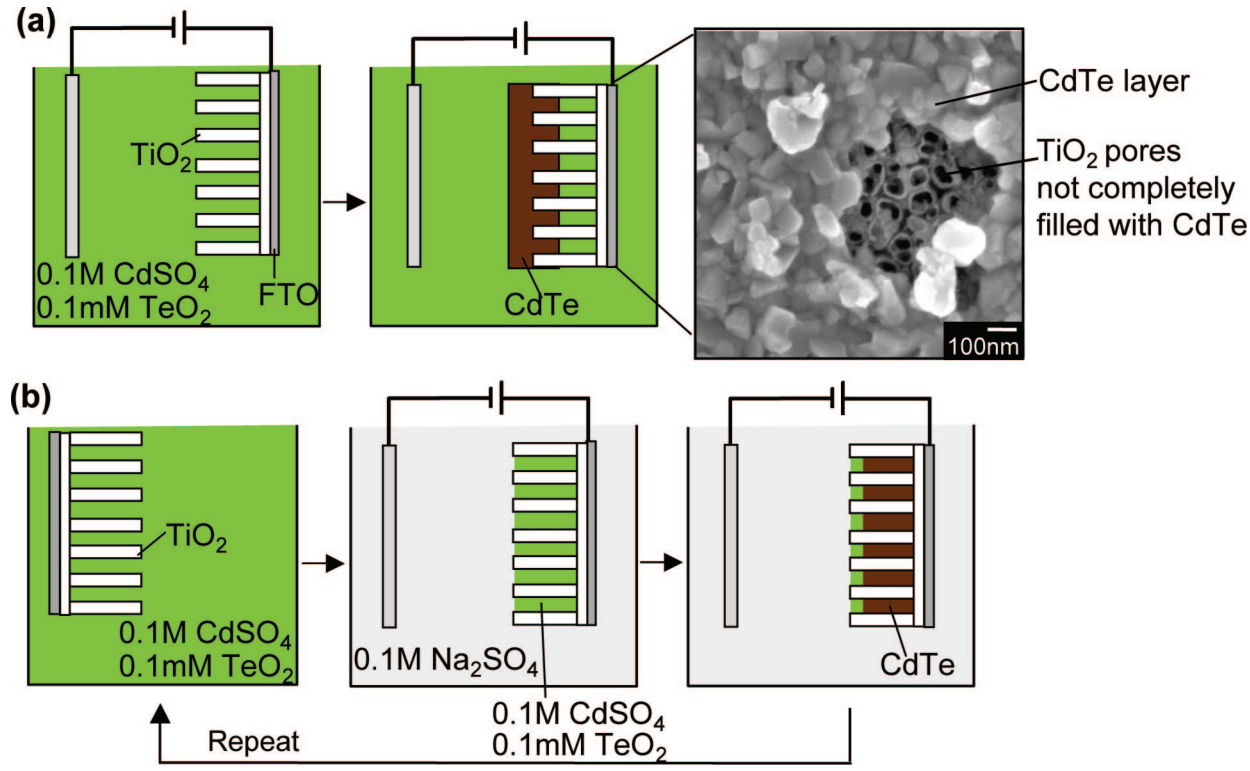

[a] An SEM image shows the presence of a thick CdTe layer deposited on TiO_2 nanotubes before the tubes are completely filled with CdTe when a regular deposition method is carried out for 1 h.

or the cathodic formation of Cd ($CdTe + 2e^- \rightarrow Cd + Te^{2-}$).[41] In contrast, the steady state photocurrent observed by the $CdTe/TiO_2$ electrode was stable, and no sign of photocorrosion was observed. We believe that this is because of the more efficient hole consumption at the electrolyte/CdTe junction and electron transfer at the $CdTe/TiO_2$ junction (from the CB of CdTe to the CB of TiO_2), achieved by enhanced electrolyte/$CdTe/TiO_2$ junction areas, which kinetically suppresses photocorrosion of the CdTe layer.

The successful CdTe photocurrent and photostability enhancement achieved by formation of a $CdTe/TiO_2$ junction prompted us to look into the possibility of improving the quality of the $CdTe/TiO_2$ junction structure. In order to make the best use of the nanotubular structures of TiO_2, it is critical that the internal area of each tube is sufficiently covered with CdTe before the entrances can become clogged. The challenge of depositing CdTe in the TiO_2 pores is that the bottom of the pores is no more conductive than the entrance of the pores, while diffusion makes deposition at the bottom of the pores less favorable than deposition at the entrance of the pores. This can result in the deposition of a thick CdTe layer on top of the pores, before a significant portion of the internal area is covered with CdTe as shown in Scheme 1a.

To overcome this problem, we developed a new technique that makes deposition in the pores more favorable than deposition on the surface of the TiO_2 nanotubes (Scheme 1b). In this technique, we utilize capillary forces to fill the pores of the TiO_2 tubes by dipping them in an electrolyte containing Cd^{2+} and $HTeO_2^+$ ions. The TiO_2 electrode is then transferred into a new medium that contains only an inert supporting electrolyte without Cd^{2+} and $HTeO_2^+$ ions. Immediate deposition after immersion in this medium results in deposition of CdTe only within the pores. This procedure can be repeated until a desired amount of CdTe is deposited in the pores.

High resolution FE-SEM images of the $CdTe/TiO_2$ films (sample I) prepared using this dipping and deposition technique after 20 repetitions are shown in Figure 6a,b. The top view shows the absence of a thick CdTe layer deposited on top of the TiO_2 pores (Figure 6a), indicating that this new method effectively suppresses deposition outside of the pores. The cross sectional SEM image confirms that CdTe is deposited successfully into the TiO_2 pores (Figure 6b). FE-SEM images of a $CdTe/TiO_2$ electrode prepared by depositing CdTe on TiO_2 tubes using a regular deposition method for 30 min (sample II) are also shown for comparison. Although the deposition time is reduced from 1 h to 30 min (compared to the sample shown in Figure 3), the resulting electrode still shows the presence of a thick CdTe layer covering the TiO_2 pores. Further, the cross sectional SEM image of sample II shows that the insides of the TiO_2 pores, especially the bottom half of the pores, are not uniformly filled with CdTe (Figure 6c,d).

Another convincing evidence showing that the dipping and deposition technique promotes deposition only in the TiO_2 pores is shown in Figure 7, which presents photographs of CdTe layers deposited on FTO substrates that contain TiO_2 nanotubes in a certain region and elsewhere expose bare FTO

(41) Elsirafy, A. A.; El-Dessouki, M. S.; El-Basiouny, M. S. *J. Electrochem. Soc.* **1987**, *134*, 221.

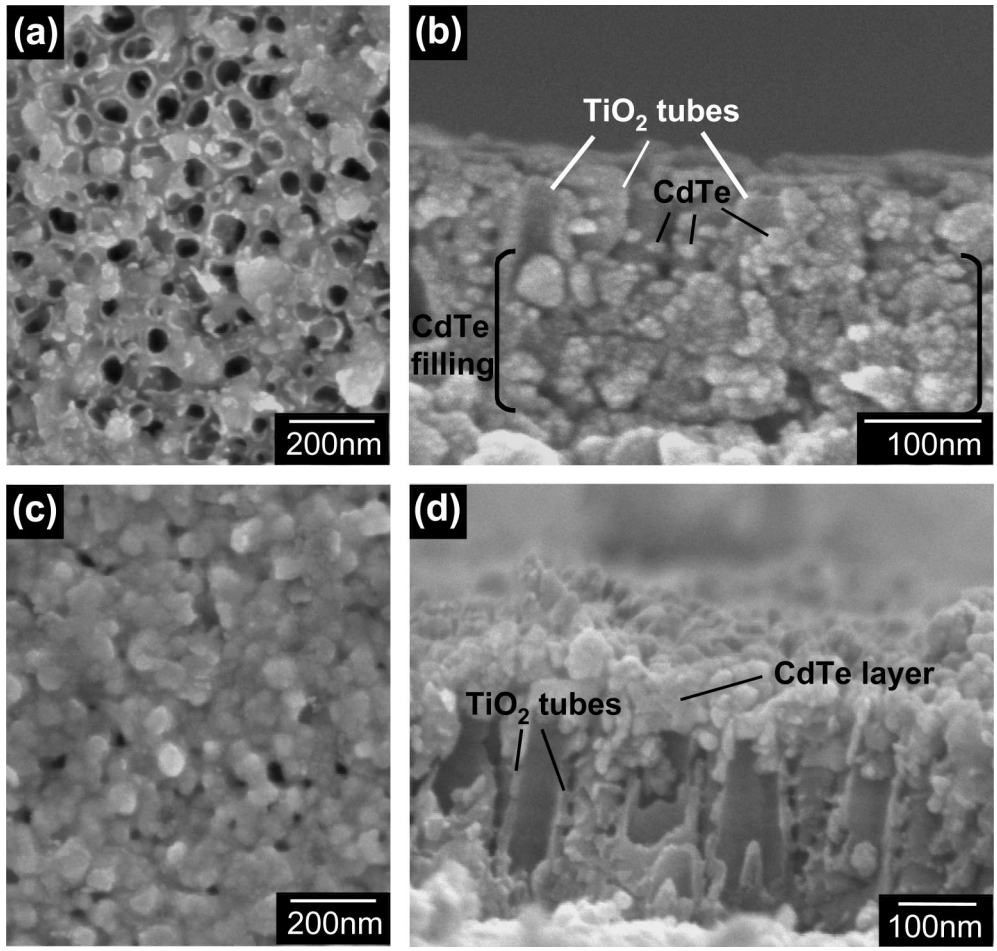

Figure 6. (a) Top and (b) side view SEM images of CdTe/TiO$_2$ electrode prepared by 20 cycles of dipping and deposition method (sample I); (c) top and (d) side view SEM images of CdTe/TiO$_2$ electrode prepared by a regular deposition method for 30 min (sample II).

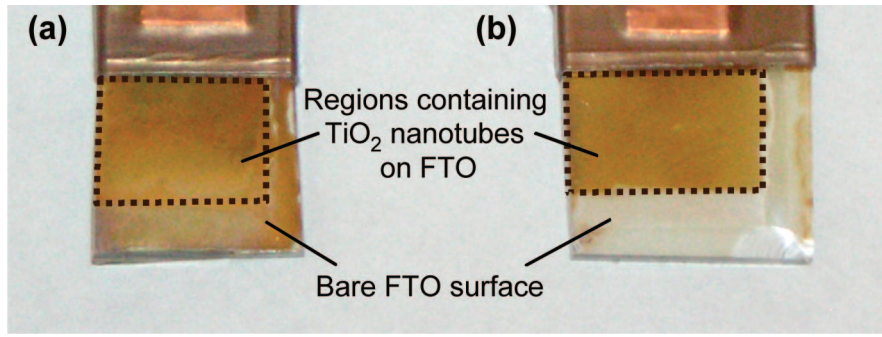

Figure 7. Photograph of CdTe films deposited on TiO$_2$ nanotube arrays using (a) a regular deposition method and (b) a new dipping and deposition technique.

surfaces. A regular deposition method resulted in deposition of CdTe both on the FTO surface and the TiO$_2$ nanotube region (Figure 7a). However, the dipping and deposition technique resulted in deposition of CdTe only within the TiO$_2$ region (Figure 7b) confirming that the new technique allows for deposition only in the TiO$_2$ pores, which were the only area of the electrode that contained the proper electrolyte. Figure 7 clearly illustrates the difference between the two deposition methods on the bulk scale, complementing the difference observed on the nanoscale by SEM studies.

The advantages of forming a high quality conformal CdTe/TiO$_2$ junction are evident when XRD patterns and UV−vis spectra of samples I and II are compared. XRD data show that sample II possessing a thick CdTe layer contains at least four times more CdTe than sample I, judging from the intensities of CdTe peaks (Figure 8). However, sample I shows a photon absorption comparable to that of sample II (Figure 9). This indicates that the CdTe layer in sample I, forming a high quality conformal coating in the TiO$_2$ pores, can efficiently increase the path length of light in the CdTe layer while decreasing the actual amount of CdTe loaded (Scheme 2). The less abrupt band gap transition observed for sample I is due to the less crystalline nature of the CdTe deposited in the TiO$_2$ nanopores when compared to the thick and continuous CdTe layer present in sample II. The difference in crystallinity is also evident in XRD patterns,

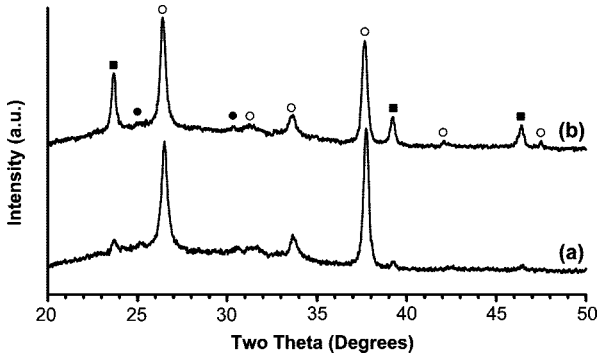

Figure 8. XRD of CdTe layers deposited on TiO_2 nanotube arrays using (a) 20 cycles of dipping and deposition (sample I) and (b) a regular deposition method for 30 min (sample II). Peaks generated from CdTe, TiO_2, and FTO are marked as (■), (●), and (○), respectively.

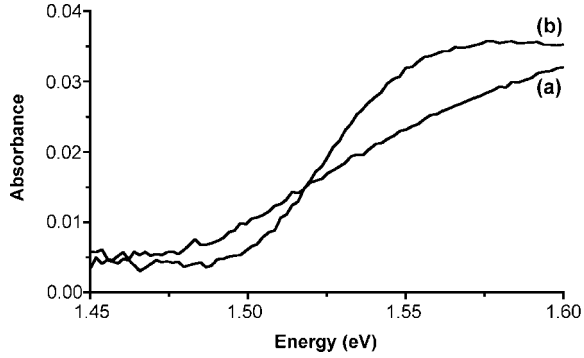

Figure 9. UV−vis spectra of CdTe layers deposited on TiO_2 nanotube arrays using (a) 20 cycles of dipping and deposition (sample I) and (b) a regular deposition method for 30 min (sample II).

where sample I shows much broader CdTe peaks (i.e., greater full width at half-maximum).

An even more interesting result was obtained when the photocurrents of sample I and sample II were compared (Figure 10). The steady state photocurrent generated by sample I (0.44 mA/cm^2) is significantly higher than that of sample II (0.19 mA/cm^2), although UV−vis spectra show that sample I induced a slightly lower photon absorption than sample II. If we assume that samples I and II generate comparable numbers of electron−hole pairs by photon absorption, this difference in photocurrent is solely due to the reduced electron−hole recombination achieved in sample

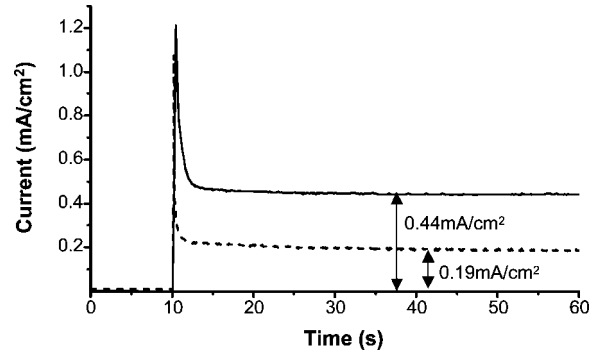

Figure 10. Short-circuit photocurrent measurement under visible light illumination of CdTe layers deposited on TiO_2 nanotube arrays using 20 cycles of dipping and deposition method (solid line) and a regular deposition method for 30 min (dashed line).

I, resulting from the formation of a more intimate CdTe/TiO_2 junction by the new deposition technique. This is because thinner and more even CdTe coating on the TiO_2 tubes allows for more efficient electron transfer at the CdTe/TiO_2 junction and hole transfer at the CdTe/electrolyte junction, minimizing electron−hole recombination in the CdTe layer. Considering that sample I contains approximately only one-fourth of the amount of CdTe that is present in sample II, the more than doubling of photocurrent observed for sample I is a significant improvement achieved simply by improving the quality of the CdTe/TiO_2 junction. This result demonstrates the necessity of forming a high quality conformal junction to fully utilize the advantages of a three-dimensionally organized junction structure. The dipping and deposition technique used in this study may be used as a general method to form a high quality conformal junction on microporous and mesoporous substrates via electrodeposition when the bottom of the pores and the entrances of the pores are equally conductive.

Conclusions

A heterojunction CdTe/TiO_2 photoelectrode was prepared by electrochemically filling tubes and tube-to-tube voids of n-type TiO_2 nanotube arrays with p-type CdTe. TiO_2 nanotube arrays used in this study were prepared by anodizing titanium films, which resulted in closely packed nanotubes with an average inner pore diameter near 50 nm,

Scheme 2. Schematic Comparison of CdTe/TiO_2 Junctions Created by (a) a Newly Developed Dipping and Deposition Technique and (b) a Regular Deposition Method[a]

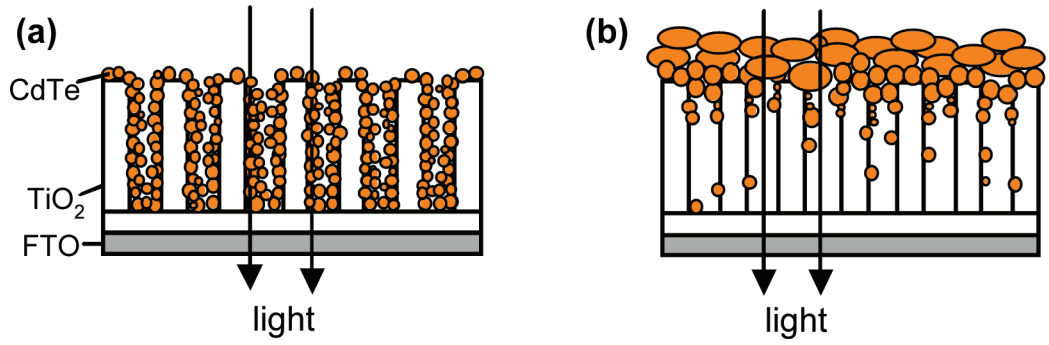

[a] The newly developed dipping and deposition technique fully utilizes internal surface areas of TiO_2 tubes and creates a more intimate CdTe/TiO_2 junction. This can significantly increase the penetration length of light without increasing the amount of CdTe deposited.

wall thickness of approximately 13 nm, and length of 250−300 nm. Cathodic deposition of CdTe on TiO_2 nanotubes resulted in the formation of a three-dimensionally structured CdTe/TiO_2 junction with significantly enhanced junction areas. The presence of the CdTe/TiO_2 junction created three major differences compared to a CdTe layer directly deposited on FTO. First, while the CdTe layer deposited on FTO showed p-type behavior and generated a cathodic photocurrent, CdTe/TiO_2 electrodes generated an anodic photocurrent, indicating that when the TiO_2/CdTe/electrolyte junction is formed, the injection of photon-generated electrons from CdTe to TiO_2 is more favored than that from CdTe to the electrolyte (i.e., polysulfide species). Second, the photocurrent generated by the CdTe/TiO_2 electrode was significantly higher than the two-dimensional CdTe layer deposited on FTO. This is because the CdTe layer deposited on the TiO_2 nanotubes possesses significantly enhanced CdTe/electrolyte and CdTe/substrate (i.e., TiO_2) junction areas that facilitate the separation of electrons and holes at the junction, thus reducing electron−hole recombination in the CdTe. Third, while the photocurrent generated by the CdTe layer alone was unstable, the CdTe deposited on the TiO_2 tubes generated stable photocurrent. This indicates that the efficient removal of photon generated electrons and holes from the CdTe layer is also beneficial for kinetically suppressing photocorrosion in the CdTe layer.

The quality of the CdTe/TiO_2 junction was improved by using a new deposition technique developed in this study, the dipping and deposition technique. This method effectively promoted deposition of CdTe within the TiO_2 nanotubes while preventing CdTe clogging at the tube entrances, enabling formation of a more intimate and conformal CdTe/TiO_2 junction. The CdTe/TiO_2 electrodes prepared by the new technique exhibited enhanced photon absorption and photocurrent generation while requiring less CdTe to be deposited in the TiO_2 tubes. These results demonstrate the importance of obtaining a good quality junction to fully utilize the advantages of a three-dimensionally organized junction structure.

The method described in this study is based on electrodeposition that allows for facile composition tuning of the CdTe layer. Considering that further improvement of CdTe-based photoelectrodes must be accompanied by the optimization of the Fermi level, band positions, and the conductivity of the CdTe layer,[42–44] the method described here will create more opportunities to improve the photoelectrochemical properties of CdTe-based photoelectrodes by enabling the formation of high quality three-dimensional junction structures as well as fine composition tuning.

Acknowledgment. This work made use of the Life Science Microscopy Facility at Purdue University. The authors wish to thank Ms. Ellen M. P. Steinmiller for assistance with FE-SEM. K.-S.C. gratefully acknowledges support of this work by the U.S. Department of Energy under Grant DE-FG02-05ER15752 and the Alfred P. Sloan foundation. C.A.G. gratefully acknowledges support of this work by the U.S. Department of Energy under Grant DE-FG02-06ER15772.

CM8010666

(42) Dobson, K. D.; Visoly-Fisher, I.; Hodes, G.; Cahen, D. *Sol. Energy Mater. Sol. Cells.* **2000**, *62*, 295–325.
(43) Sahu, S. N.; Antonio, M. J.; Sanchez, C. *Sol. Energy Mater. Sol. Cells* **1996**, *43*, 223–235.
(44) Ghosh, S.; Purakayastha, P. K.; Datta, R. W.; Miles, M. J.; Carter, R. H. *Semicond. Sci. Technol.* **1995**, *10*, 71–76.